# Vacuum-ultraviolet spectroscopy of Xe: Hyperfine splittings, isotope shifts, and isotope-dependent ionization energies

F. Brandi, I. Velchev, W. Hogervorst, and W. Ubachs
*Laser Centre, Department of Physics and Astronomy, Vrije Universiteit, De Boelelaan 1081, 1081 HV Amsterdam, The Netherlands*
(Received 30 October 2000; revised manuscript received 28 March 2001; published 16 August 2001)

High-resolution spectroscopy of xenon is performed on four transitions from the $5p^6\,{}^1S_0$ ground state to the $5d'[3/2]_1$, $8d[1/2]_1$, $8d[3/2]_1$, and $7s'[1/2]_1$ excited states ($jl$-coupling notation) by means of 1VUV $+$1UV photoionization spectroscopy. Spectra of all nine stable isotopes are resolved enabling the determination of the hyperfine splittings and isotope shifts. Magnetic dipole (for both $^{129}$Xe and $^{131}$Xe) and electric quadrupole (for $^{131}$Xe) hyperfine splitting constants are derived for all four excited states. Mass and field shift contributions to the isotope shifts are separated using King plots relative to existing accurate isotope shift values. A high field shift factor, even for the transitions in which no *s* electron is involved, is deduced. From precise calibration of the transition frequencies an accurate value for the ionization energy of $^{136}$Xe, $E_{3/2}^{136} = 97\,833.805(11)\ \mathrm{cm}^{-1}$, is derived. In addition, values of the ionization energies for all other isotopes are determined.

DOI: 10.1103/PhysRevA.64.032505 PACS number(s): 32.10.Hq, 32.10.Fn, 32.30.Jc

## I. INTRODUCTION

High-resolution laser spectroscopy involving the ground state of noble gases requires a tunable narrow-band light source in the vacuum-ultraviolet (VUV) range because of the large energy gap to the excited states. Nowadays, the use of pulsed-dye amplification of a tunable cw laser light source, followed by nonlinear up-conversion processes, allows for the production of coherent VUV light. Such a source, in combination with the technique of 1VUV+1UV photoionization, has already been applied to spectroscopic investigations of the noble gases He, Ne, Ar, and Kr [1–4], in which isotope shifts (IS's) and hyperfine splittings (HFS's) could be measured. For He and Ar new and accurate values of the ionization energy have been deduced from these measurements. For the heaviest stable noble gas, xenon, accurate values for the VUV transitions from the ground state are missing; hence the ionization energy is less accurately known.

Here we present the results of high-resolution 1VUV $+$1UV photoionization spectroscopy in Xe. We investigate the transitions from the ground state $5p^6$ to four excited states: $5d'[3/2]_1$, $8d[1/2]_1$, $8d[3/2]_1$, and $7s'[1/2]_1$ ($jl$-coupling notation) at 106.8, 106.1, 105.6, and 104.4 nm, respectively. Natural xenon contains nine stable isotopes with abundances $^{124}$Xe (0.0096%), $^{126}$Xe (0.009%), $^{128}$Xe (1.92%), $^{129}$Xe (26.4%), $^{130}$Xe (4.1%), $^{131}$Xe (21.1%), $^{132}$Xe (26.9%), $^{134}$Xe (10.4%), and $^{136}$Xe (8.9%). Our setup allows us to spectrally resolve all isotopes and to measure the IS in the investigated transitions. The two odd isotopes possess nonzero nuclear spin ($I^{129} = 1/2, I^{131} = 3/2$), inducing hyperfine splitting of the $J=1$ excited states. The hyperfine structures are fully resolved and HFS constants determined.

The investigation of the IS's of heavy elements can provide insight in the electronic density at the nucleus. Previous IS measurements in a two-photon transition from the ground state of xenon [5] seem to indicate a large screening effect by the *p* electrons in the closed shell.

Absolute transition frequencies are measured using a calibration procedure based on saturation spectroscopy of molecular iodine and use of an actively stabilized Fabry-Pérot interferometer. Our work connects, by means of accurate frequency measurements, the energy of the ground state to the entire manifold of electronically excited states; transitions between those excited states, and their position with respect to the ionization limit, have been studied elsewhere with high accuracy. The combination of the present and existing data results in our accurate determination of isotope-dependent ionization energies in xenon.

## II. EXPERIMENT

The experimental apparatus to generate wavelength-tunable VUV pulses has been presented previously [3]; here only a brief description will be given. cw light from a tunable ring-dye laser (Spectra Physics 380), running on DCM dye and pumped with the second harmonic of a cw Nd:$YVO_4$ laser (Millennia, Spectra Physics), is amplified in a three-stage pulse-dye amplifier (PDA). The PDA, which also operates on DCM dye and is pumped by the second harmonic of an injection-seeded *Q*-switched Nd:YAG laser, delivers pulses with a repetition rate of 10 Hz, duration of 5 ns, and energy up to 60 mJ. These pulses are then frequency doubled in a KD*P crystal, producing pulses of 8 mJ in the UV, and subsequently focused in a xenon gas jet for third harmonic generation.

The overlapping UV and VUV light beams intersect at 90° a collimated xenon atomic beam in the interaction region, where a 1VUV+1UV photoionization process is induced. On resonance the time-of-flight mass spectrometer collects the ions to be detected on an electron multiplier. The signal from each isotope is recorded with different boxcar integrators, whose gates are set at appropriate time windows. The signal-to-noise ratio is sufficient to reveal also the less abundant $^{124}$Xe and $^{126}$Xe isotopes, except for the case of the weakest transition to the $8d[1/2]_1$ excited state.

The absolute frequency of the cw light is calibrated by

 

simultaneous recording of a saturated absorption spectrum of molecular iodine. The *t* hyperfine components of the $I_2$ lines, recently calibrated with 1 MHz accuracy ($1\sigma$) in the 595–655 nm wavelength range [6], are used as a reference. Calibration of the VUV light is accomplished taking into account the factor of 6 due to the frequency doubling and tripling. The center frequency of the pulsed output of the PDA may undergo, because of chirp, a small net shift with respect to the seeding cw light, used for calibration. This issue, including its effect on the harmonic frequencies, has been extensively discussed elsewhere [1,7]. From such studies it is estimated that the uncertainty in the absolute VUV frequency is less than 0.003 $cm^{-1}$. The chirp phenomenon does not affect the results of relative frequency measurements, such as isotope shifts and hyperfine splittings.

In addition, the transmission peaks of a Fabry-Pérot interferometer (FPI) are also recorded, in order to obtain accurate frequency markers for the cw light. The FPI is locked to a frequency-stabilized He-Ne laser, and its free spectral range of 148.9563(3) MHz is calibrated against the known *t* hyperfine component of two $I_2$ lines [$P65(7\text{-}4)$ and $P95(7\text{-}4)$ [6]]. The FPI fringes are then translated into VUV frequency markers with a spacing of 893.7378(18) MHz. Spectra of the xenon resonances, the $I_2$ reference spectrum, and the FPI markers are stored in a computer for further analysis. The width of the xenon lines is typically 400 MHz (full width at half maximum) in a Gaussian profile, mainly arising from the bandwidth of the VUV light and a small Doppler contribution in the crossed-beam configuration.

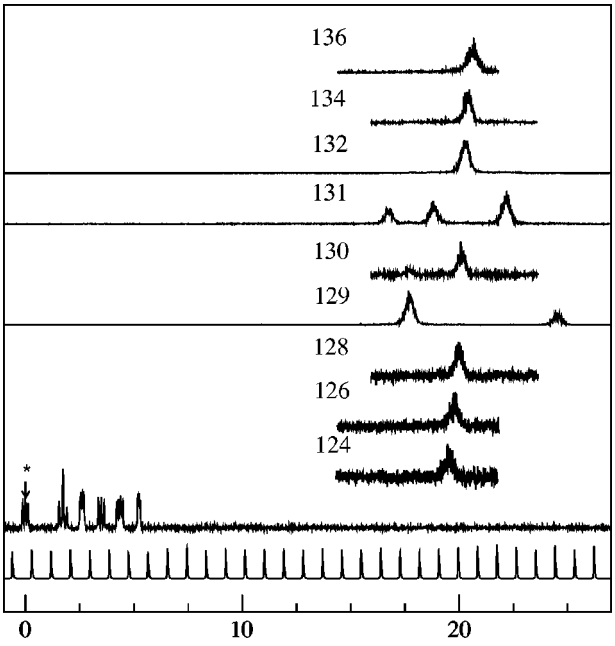


FIG. 1. Spectra of the ($5p^6$-$7s'[1/2]_1$) transition, for all natural isotopes of xenon indicated by their mass number; FPI transmission peaks, from which the frequency scale was deduced, are also shown; the zero frequency has been set at the *t* hyperfine component of the $R95(10-4)$ $I_2$ line (denoted by *) used for absolute frequency calibration; this zero is in fact at 2 872 009.06 GHz.

## III. RESULTS AND DISCUSSION

The four transitions investigated are indicated by their excited state configurations, namely, $5d'[3/2]_1$, $8d[1/2]_1$, $8d[3/2]_1$, and $7s'[1/2]_1$. Isotopically and hyperfine resolved spectra of these states in excitation from the ground state are recorded. An example of the experimental results is given in Fig. 1, where spectra recorded for all nine isotopes in the $7s'[1/2]_1$ transition are shown. The different noise levels in the spectra reflect the relative natural abundance of the isotopes. Since only four boxcars are used not all the isotopic lines can be measured simultaneously; hence one isotopic signal is chosen as reference and recorded in each scan to facilitate the data analysis. Figure 1 contains the results of three different scans, which are put together on the same frequency scale making use of the signal from the reference isotope. The FPI marks are also shown and the frequency scale is given in VUV frequency. It has to be noted that the weak peak present in the $^{130}$Xe spectrum is an artifact, associated with the resonance of the highly abundant $^{129}$Xe. To perform the absolute frequency calibration a long scan is usually needed to bridge the gap between the xenon line and the nearest $I_2$ line. In the case of $7s'[1/2]_1$ the gap toward the $R95(10-4)$ line is $\sim 20$ GHz. In the following sections the results of the measurements are presented and discussed.

### A. Hyperfine splitting

Hyperfine splitting in an atomic energy level is due to the interaction of the magnetic and electric multipole moments of the nucleus with the electrons and exists only for electronic configurations with angular momentum $J \neq 0$. The strongest effects arise from interactions with the magnetic dipole and the electric quadrupole moments of the nuclear charge distribution, the latter being present only for nuclear spin $I > 1/2$. When these two contributions are considered, the HFS between two adjacent hyperfine components is given by [8]

$$\Delta_{F,F-1} = AF + \frac{3}{2}BF\frac{F^2+\frac{1}{2}-I(I+1)-J(J+1)}{I(2I-1)J(2J-1)}, \tag{3.1}$$

where $F$ is the total angular momentum of the atom and $A$ and $B$ are the magnetic dipole and electric quadrupole hyperfine constants, respectively. Since ground states of noble gases have $J=0$, measured splittings directly reflect the HFS of the excited state.

The measured hyperfine splittings are presented in Table I. They are averaged over 4 to 12 spectra, depending on the number of scans recorded for each individual line, while the quoted uncertainties represent the standard deviation. The individual hyperfine components are identified on the basis of the intensity rule [8], i.e., higher intensity for larger $F$ values. From the HFS's reported in Table I and using Eq. (3.1), it is possible to derive the hyperfine constants $A$ and $B$, also included in Table I. In the $^{129}$Xe isotope there is no quadrupole term since $I^{129}=1/2$.

TABLE I. Results of hyperfine splitting measurements. All values are in MHz and reported uncertainties are $1\sigma$.

| | $5d'[3/2]_1$ | $8d[1/2]_1$ | $8d[3/2]_1$ | $7s'[1/2]_1$ |
|---|---|---|---|---|
| $\Delta^{131}_{5/2,3/2}$ | −1200(18) | 328(19) | −625(30) | 3336(9) |
| $\Delta^{131}_{3/2,1/2}$ | −797(23) | 398(14) | −467(20) | 2063(17) |
| $A^{131}$ | −493(7) | 165(10) | −265(10) | 1345(4) |
| $B^{131}$ | 26(8) | −67(6) | 31(9) | −20(6) |
| $\Delta^{129}_{3/2,1/2}$ | 2486(18) | −869(9) | 1369(34) | −6822(23) |
| $A^{129}$ | 1657(12) | −579(6) | 913(23) | −4548(15) |

A consistency check for the HFS measurements involves evaluation of the ratio $A^{129}/A^{131}$. The magnetic dipole constant $A$ is proportional to the ratio of the nuclear magnetic moment $\mu$ and the nuclear spin; hence $A^{129}/A^{131} = \mu^{129}I^{131}/\mu^{131}I^{129}$. Using $\mu^{129} = -0.7768\mu_N$ and $\mu^{131} = 0.6908\mu_N$ ($\mu_N$ is the nuclear magneton) this ratio becomes $A^{129}/A^{131} = -3.373$. The values of $A^{129}$ and $A^{131}$ reported in Table I show that, within the error margins, the experimental ratio $A^{129}/A^{131}$ is compatible with this value.

### B. Isotope shift

The IS of an atomic transition contains two different contributions. One is related to the finite mass of the nucleus and is commonly referred to as the mass shift (MS), while the other is due to the nonzero size of the nucleus and is called the field shift (FS) [9]. The latter is predominant in heavy elements ($Z>60$), while the former prevails in light elements ($Z<30$). For a medium-weight element like xenon both effects give a significant contribution.

Formally, the isotope shift in an atomic transition $i$ is the difference between the transition frequency $\nu_i$ of two isotopes with mass numbers $A'$ and $A$, $\Delta_i^{A',A} = \nu_i^{A'} - \nu_i^{A}$. It can be expressed as [10]

$$\Delta_i^{A',A} = \Delta_{MS,i}^{A',A} + \Delta_{FS,i}^{A',A} = M_i \frac{A'-A}{AA'} + F_i \lambda^{A',A}. \quad (3.2)$$

The mass shift factor is conventionally separated into two terms, $M_i = M_{N,i} + M_{S,i}$. The first term describes the so-called normal mass shift, which represents the contribution of the reduced mass of the electron in the atomic system and is given to a good approximation by $(m_e/m_u)\nu_i$, where $m_e$ and $m_u$ are the electron mass and atomic mass unit, respectively. The second term describes the specific mass shift that arises from the correlated electron momenta. Its evaluation requires complicated many body atomic structure calculations.

The field shift factor $F_i$ is proportional to the change in the total electron density at the nucleus when the atom undergoes the atomic transition $i$, while the nuclear parameters $\lambda^{A',A}$ are given, to a good approximation, by the change in the mean-square nuclear charge radius between isotopes.

The measured IS's are presented in Table II. The heaviest $^{136}$Xe isotope is chosen as a reference to express the isotope shifts. The reported values are averaged over 4 to 18 measurements depending on the number of scans recorded for each isotope, while errors are $1\sigma$. In the weaker $8d[1/2]_1$ transition the two less abundant $^{126}$Xe and $^{124}$Xe isotopes are not observed.

TABLE II. Results of isotope shift measurements $\Delta_i^{136,A} = \nu_i^{136} - \nu_i^{A}$ (in MHz). Reported uncertainties are $1\sigma$.

| $A$ | $5d'[3/2]_1$ | $8d[1/2]_1$ | $8d[3/2]_1$ | $7s'[1/2]_1$ |
|---|---|---|---|---|
| 134 | 203(10) | 207(12) | 219(15) | 213(12) |
| 132 | 351(18) | 384(18) | 354(20) | 365(18) |
| 131 | 470(11) | 531(23) | 545(17) | 492(20) |
| 130 | 509(13) | 557(11) | 529(30) | 523(24) |
| 129 | 591(19) | 675(14) | 684(27) | 678(24) |
| 128 | 667(12) | 747(19) | 726(20) | 692(22) |
| 126 | 821(14) | | 912(20) | 869(25) |
| 124 | 1008(20) | | 1116(20) | 1069(22) |

For the two odd isotopes the IS's are evaluated from the center of gravity of the measured HFS. According to the ''odd-even staggering'' phenomenon they do not lie midway between the two neighboring even isotopes, but closer to the lighter one [11]. This is graphically shown in Fig. 2, where the measured $\Delta^{136,A}_{8d[3/2]_1}$ and $\Delta^{136,A}_{7s'[1/2]_1}$ are plotted against the atomic mass number $A$. Figure 2 also shows the anomaly for $^{136}$Xe, related to the neutron shell closing at $N=82$. These effects reflect the behavior of the change in the mean-square nuclear charge radius between isotopes. In our analysis attention will be focused on interpretation of the IS with the aim of extracting information on the electronic structure of the atom. This implies that all the information on the nuclear charge distribution, contained in the nuclear parameters $\lambda^{A',A}$, will be divided out, leaving only the effect of the electronic structure, contained in the $M_i$ and $F_i$ factors.

In order to extract physical information from the measured IS's we perform the well known King plot analysis [9]. To do so we introduce the so-called ''modified IS'' defined as $\Delta_i^{A',A}$ divided by the atomic mass factor $(A'-A)/AA'$.

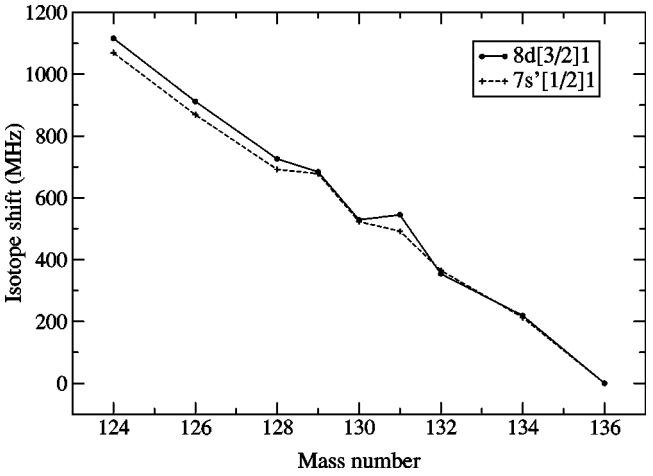


FIG. 2. Measured isotope shift as a function of the mass number, for the $8d[3/2]_1$ and $7s'[1/2]_1$ transitions. The experimental uncertainty is about 20 MHz.

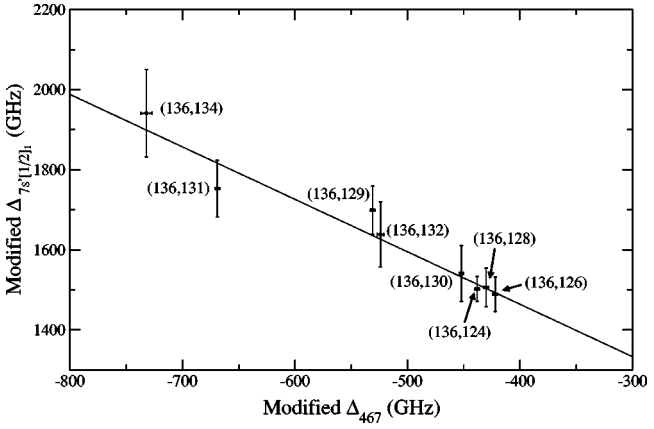


FIG. 3. King plot between $\Delta^{136,A}_{7s'[1/2]_1}$, measured in the present work, and $\Delta^{136,A}_{467}$, reported in [12]. The isotope pair is specified for each point; the straight line is the result of a weighted linear least-squares fit.

Then, when two transitions $i,j$ are considered, it follows from Eq. (3.2) that the corresponding modified IS's obey the following linear relation:

$$\Delta_i^{A',A}\frac{AA'}{A'-A}=\left(\frac{F_i}{F_j}\right)\Delta_j^{A',A}\frac{AA'}{A'-A}+\left(M_i-\frac{F_i}{F_j}M_j\right). \tag{3.3}$$

When the modified IS's of the two transitions belonging to the same isotope pair are plotted one against the other (King plot) the slope and intercept deduced from a linear least-squares fit give, respectively, $(F_i/F_j)$ and $[M_i-(F_i/F_j)M_j]$. It is worth noting that if $\Delta_j^{A',A}$ are known then, through Eq. (3.3), it is possible to evaluate $\Delta_i^{A',A}$ for all isotope pairs once they are known for at least two isotope pairs.

To take the maximum advantage of our data we perform King plots relative to the modified IS's in the $(6s[3/2]_2-7p[5/2]_3)$ transition at 467 nm $(j=467)$ measured by Schneider [12]. These data are very accurate, with an uncertainty less than 1 MHz, and cover all the natural isotopes of xenon. As an example, in Fig. 3 the modified $\Delta^{136,A}_{7s'[1/2]_1}$ vs modified $\Delta^{136,A}_{467}$ plot is shown along with the straight line resulting from a weighted linear least-squares fit in which the statistical errors on our data are used as weight. Such a fit is performed for every transition and the results are presented in the first two rows of Table III where the reported uncertainty arises from the fit procedure.

Absolute values of the isotope shift factors cannot be extracted from King plots unless they are known for one of the transitions [see Eq. (3.3)]. The main result of our IS measurements follows from the relative $F_i/F_{467}$ values obtained; a high value for the field shift factors is deduced even for those transitions in which no $s$ electron is involved. This is consistent with the result of the first IS measurement in a transition involving the ground state of xenon as performed by Plimmer *et al.* [5]. They measured the IS in the two-photon transition between the ground state and the $6p[1/2]_0$ excited state, and deduced a value for $F_{6p[1/2]_0}/F_{467}$ of $-1.207(11)$. This effect is ascribed to an increase in the electron density at the nucleus that results from the removal of a $5p$ electron from the closed shell configuration, thereby strongly decreasing the screening of the inner $s$ electrons.

In order to give an estimate of the $F_i$ and $M_i$ factors for the investigated transitions we use the values of the isotope shift factors given by Schneider for the 467 nm transition [12] (see also [13]). The $F_{467}$ factor is evaluated using the relation $F_{(ns\text{-}n'p)}=(\pi a_0^3/Z)|\Psi(0)|^2_{ns}\beta f(Z)$ [9], where $a_0$ is the Bohr radius, $|\Psi(0)|^2_{ns}$ the nonrelativistic $ns$ electron density at the nucleus, $\beta$ the screening factor, for which a value 1.16 follows from a Hartree-Fock calculation on the $6s$ configuration, and $f(Z)$ the relativistic correction [$f(54)=11.37$ GHz fm$^{-2}$]. The quantity $(\pi a_0^3/Z)|\Psi(0)|^2_{ns}$ is estimated by two methods involving both the Goudsmit-Fermi-Segrè formula and the magnetic hyperfine splitting constant, from which $F_{467}=2.06$ GHz fm$^{-2}$ is deduced. Based on empirical methods, in particular related to critically evaluated data on the Ba chain, Schneider estimates the specific mass shift to be $-56(10)$ MHz for the (136,134) isotope pair, from which $M_{467}=-158(91)$ GHz is obtained. Estimates for the absolute values of $F_i$ and $M_i$ factors pertaining to the four transitions investigated here are given in the last two rows of Table III. However it has to be pointed out that in general there is not a unique and reliable estimate for the specific mass shift (see [10,13]); consequently the value of $M_{467}$, and those of $M_i$ reported in Table III, have to be interpreted with caution. In contrast the values obtained for the $F_i$ factors are fairly reliable since the method used to evaluate the field shift factor for $(ns\text{-}n'p)$ transitions is generally accepted.

### C. Absolute calibration

Absolute calibration of the resonance frequency is performed on three transitions, $8d[1/2]_1$, $8d[3/2]_1$, and $7s'[1/2]_1$, for which the results are reported in Table IV. The

TABLE III. Result of King plots; the absolute values of $F_i$ and $M_i$ are obtained using the estimate $F_{467}=2.06$ GHz fm$^{-2}$ and $M_{467}=-158(91)$ GHz reported in [12].

| | | $5d'[3/2]_1$ | $8d[1/2]_1$ | $8d[3/2]_1$ | $7s'[1/2]_1$ |
|---|---|---|---|---|---|
| $F_i/F_{467}$ | | $-1.12(15)$ | $-0.94(26)$ | $-1.48(23)$ | $-1.31(23)$ |
| $M_i-(F_i/F_{467})M_{467}$ | (GHz) | 950(71) | 1211(130) | 927(107) | 940(112) |
| $F_i$ | (GHz fm$^{-2}$) | 2.31(32) | 1.94(54) | 3.05(47) | 2.70(47) |
| $M_i$ | (GHz) | 1127(126) | 1360(161) | 1161(176) | 1147(168) |

TABLE IV. Absolute calibration of transition frequencies from the ground state (values in $cm^{-1}$). The first and second rows denote the reference Xe isotope and the $I_2$ reference line. $\nu^{I_2}$ is the frequency of the *t* hyperfine component of this $I_2$ line, $\Delta\nu^{A_{ref},I_2}$ is the measured frequency difference between the reference xenon isotope line and this *t* component in the VUV frequency scale, and $\nu^{A_{ref}}$ is the absolute frequency of the xenon line for the reference isotope. In the last row values from Yoshino and Freeman [14] are given.

| | $8d[1/2]_1$ | $8d[3/2]_1$ | $7s'[1/2]_1$ |
|---|---|---|---|
| $A_{ref}$ | 136 | 136 | 132 |
| $I_2$ | *P*30(7-4) | *P*68(8-4) | *R*95(10-4) |
| $\nu^{I_2}$ | 15704.88007(3) | 15780.92844(3) | 15966.65174(3) |
| $\Delta\nu^{A_{ref},I_2}$ | −1.2617(12) | −0.08839(57) | 0.67629(61) |
| $\nu^{A_{ref}}$ | 94228.0187(32) | 94685.4822(30) | 95800.5867(30) |
| From [14] | 94228.02(20) | 94685.47(20) | 95800.70(20) |

frequencies of the *t* hyperfine component of the $I_2$ lines, $\nu^{I_2}$, are taken from the new atlas of reference lines [6]. The measured values for the frequency difference between the reference Xe isotope line and the *t* component of the $I_2$ calibration line, $\Delta\nu^{A_{ref},I_2}$, are given on a VUV frequency scale (see Fig. 1). These are averaged values from 5 to 8 measurements, depending on the number of spectra recorded; the uncertainties represent $1\sigma$. The absolute frequency for the reference Xe isotope line is obtained as $\nu^{A_{ref}}=\Delta\nu^{A_{ref},I_2}+6\times\nu^{I_2}$, where the factor 6 reflects the fact that the $I_2$ saturated absorption lines are measured with the fundamental frequency. The uncertainty in $\nu^{A_{ref}}$ is due to the experimental errors in $\Delta\nu^{A_{ref},I_2}$ plus a possible contribution due to frequency chirp arising in the PDA. This is estimated to be less than 0.003 $cm^{-1}$ [1,7] and is the main source of error in the absolute calibration. Previous results from classical absorption spectroscopy [14] are reported for comparison in the last row of Table IV. However, here no isotope is specified since the individual isotope lines were not resolved. The present results are fully consistent with previous data and increase the accuracy by almost two orders of magnitude.

From the absolute calibration of the $8d[1/2]_1$ transition it is possible to derive a more accurate value of the ionization energy of $^{136}$Xe. Knight and Wang [15] performed laser spectroscopy of the $nf[3/2]_1$ ($n>24$) Rydberg series in Xe, resulting in an ionization limit of 21 637.02(1) $cm^{-1}$ from the $6s'[1/2]_0$ level. A value of the ionization energy of $E_{3/2}=97\,833.81(10)$ $cm^{-1}$ was reported as well, based on the value of the energy of the $6s'[1/2]_0$ level of 76 196.79(10) $cm^{-1}$. However, from the high-precision interferometric measurements on enriched $^{136}$Xe sample by Humphreys and Paul [16], an energy separation between $6s'[1/2]_0$ and $8d[1/2]_1$ levels of 18 031.2339(14) $cm^{-1}$ can be deduced. This value, combined with the absolute calibration of the energy of the $8d[1/2]_1$ level in $^{136}$Xe, gives an energy of the $6s'[1/2]_0$ level of 76 196.7848(35) $cm^{-1}$. Finally, a value for the ionization energy for $^{136}$Xe of $E_{3/2}^{136}=97\,833.805(11)$ $cm^{-1}$ results. The energy levels involved in the evaluation of the ionization energy are schematically shown in Fig. 4.

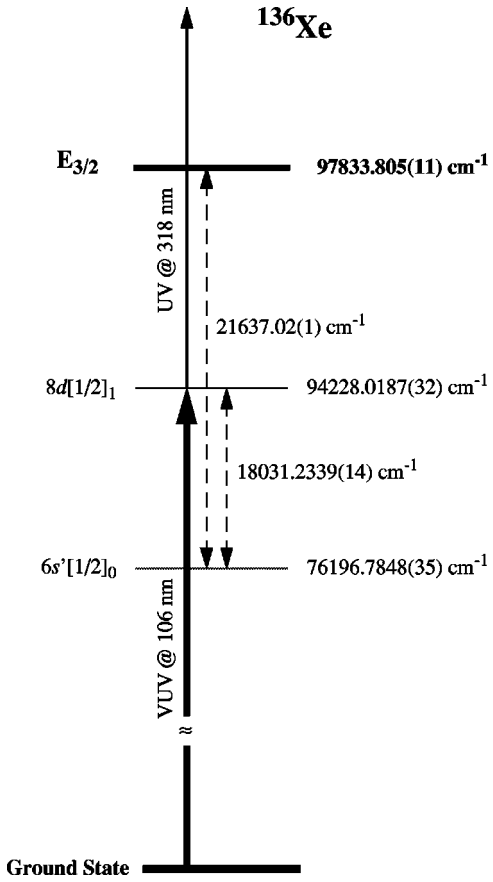


FIG. 4. Scheme of the energy levels involved in the evaluation of the ionization energy of $^{136}$Xe; the continuous arrows represent the VUV and UV photons used in the spectroscopic measurements reported in this work, from which the energy of the $8d[1/2]_1$ level has been determined; the dashed arrows indicate the energy separations reported in the literature: first the energy separation between the $6s'[1/2]_0$ and $8d[1/2]_1$ levels from [16] is used to evaluate the energy of the $6s'[1/2]_0$ level and then the ionization energy is estimated using the ionization limit from the $6s'[1/2]_0$ level reported in [15].

It has to be pointed out that in the experiment of Knight and Wang [15] isotopic lines were not resolved, so that, to validate the present result, an estimate has to be given of the IS's in the transitions measured. Using the results reported by Jackson and Coulombe [17] of $\Delta^{136,130}_{(6s'[1/2]_0-5f[3/2]_1)}=-84(9)$ MHz, an upper limit of 0.003 $cm^{-1}$ for the IS between $^{136}$Xe and $^{130}$Xe in the transitions studied in [15] can be estimated. This shift does not affect the result for the ionization energy of $^{136}$Xe at the present level of accuracy.

Another relevant fact that can be deduced from data reported in the literature is the IS between the ground state (GS) and the $6s'[1/2]_0$ excited state, from which an estimate of the isotope-dependent ionization energies can be derived. To do so the following identity is used:

$$\Delta^{A',A}_{(GS\text{-}6s'[1/2]_0)}=\Delta^{A',A}_{(GS\text{-}6p[1/2]_0)}-\Delta^{A',A}_{(6s[3/2]_1\text{-}6p[1/2]_0)}+\Delta^{A',A}_{(6s[3/2]_1\text{-}6s'[1/2]_0)}. \quad (3.4)$$

TABLE V. Summary of the isotope-dependent ionization energies $E^A_{3/2}$. The first column gives the ionization energy of $^{136}$Xe ($E^{136}_{3/2}$) in cm$^{-1}$, with uncertanty of 0.011 cm$^{-1}$, while the others give $\Delta^{136,A}_{(GS\text{-}6s'[1/2]_0)}$ (in $10^{-3}$cm$^{-1}$). From these data the isotope-dependent ionization energies can be evaluated as $E^A_{3/2}=E^{136}_{3/2}-\Delta^{136,A}_{(GS\text{-}6s'[1/2]_0)}$.

| $E^{136}_{3/2}$ | 134 | 132 | 131 | 130 | 129 | 128 | 126 | 124 |
|---|---|---|---|---|---|---|---|---|
| 97833.805 | 9.0 | 15.0 | 21.7 | 21.2 | 27.2 | 28.4 | 35.5 | 44.0 |

The values of the first term on the right hand side are given by Plimmer *et al.* [5], while for the second term values were measured by Jackson and Coulombe [18]. To evaluate the third term, values reported also in [18] for the IS's in $(6s'[1/2]_0\text{-}7p[3/2]_1)$, $(6s[3/2]_1\text{-}7p[3/2]_1)$, $(6s'[1/2]_0\text{-}6p'[3/2]_1)$, and $(6s[3/2]_1\text{-}6p'[3/2]_1)$ transitions are used to derive two sets of values for $\Delta^{A',A}_{(6s[3/2]_1\text{-}6s'[1/2]_0)}$. These are consistent within the error margins and the weighted mean is assumed. However, no direct evaluation of the IS in the $(GS\text{-}6s'[1/2]_0)$ transition is possible for $^{124}$Xe, $^{126}$Xe, $^{129}$Xe, and $^{131}$Xe, since no measurements were reported for these isotopes in Ref. [18]. Nevertheless a King plot with respect to the 467 nm transition allows one to evaluate $\Delta^{A',A}_{(GS\text{-}6s'[1/2]_0)}$ for these isotopes also.

A summary of the results on the isotope-dependent ionization energies is given in Table V. In the first column the ionization energy of $^{136}$Xe is reported. In the others the evaluated $\Delta^{136,A}_{(GS\text{-}6s'[1/2]_0)}$ are given in units of $10^{-3}$ cm$^{-1}$, with uncertanty of $0.4\times10^{-3}$ cm$^{-1}$. If the isotope shifts in the $(6s'[1/2]_0\text{-}nf[3/2]_1)$ transitions are considered (see above), the $\Delta^{136,A}_{(GS\text{-}6s'[1/2]_0)}$ values give an estimate of the ionization energy differences with an accuracy of about 0.003 cm$^{-1}$. In view of this, the isotope-dependent ionization energies can be estimated as, $E^A_{3/2}=E^{136}_{3/2}-\Delta^{136,A}_{(GS\text{-}6s'[1/2]_0)}$.

## IV. CONCLUSIONS

In this article results of high-resolution VUV-laser spectroscopy of xenon are presented. Tunable narrow-band VUV pulses near 105 nm wavelength are used to investigate transitions from the ground state to four excited states $5d'[3/2]_1$, $8d[1/2]_1$, $8d[3/2]_1$, and $7s'[1/2]_1$ by two-step ionization spectroscopy. A time-of-flight mass spectrometer allows resolution of the transitions of all nine stable isotopes; isotope shifts and hyperfine splittings can be measured. Values for the hyperfine splitting constants are derived for the $^{129}$Xe and $^{131}$Xe isotopes. Using King plots field shift and mass shift contributions are separated. The field factor turns out to be high, even when no *s* electron is involved in the transition. This result confirms observations made by Plimmer *et al.* [5], that the removal of a *p* electron from the ground state's closed shell configuration strongly increases the electronic density at the nucleus.

For three of the transitions an absolute frequency calibration is also performed. This results in a two orders of magnitude higher accuracy for the absolute energies of the investigated levels compared with previous measurements. A value for the ionization energy of $^{136}$Xe is derived with an accuracy of about one order of magnitude better then the previous value. Finally, using isotope shift measurements reported in the literature, isotope-dependent ionization energies for all Xe isotopes are derived.


[1] K.S.E. Eikema, W. Ubachs, W. Vassen, and W. Hogervorst, Phys. Rev. A **55**, 1866 (1997).

[2] K.S.E. Eikema, W. Ubachs, and W. Hogervorst, Phys. Rev. A **49**, 803 (1994).

[3] I. Velchev, W. Hogervorst, and W. Ubachs, J. Phys. B **32**, L511 (1999).

[4] T. Trickl, M.J.J. Vrakking, E. Cromwell, Y.T. Lee, and A.H. Kung, Phys. Rev. A **39**, 2948 (1989).

[5] M.D. Plimmer, P.E.G. Baird, C.J. Foot, D.N. Stacey, J.B. Swan, and G.K. Woodgate, J. Phys. B **22**, L241 (1989).

[6] S.C. Xu, R. van Dierendonck, W. Hogervorst, and W. Ubachs, J. Mol. Spectrosc. **201**, 256 (2000).

[7] E.E. Eyler, A. Yiannopoulou, S. Gangopadhyay and N. Melikechi, Opt. Lett. **22**, 49 (1997).

[8] H. Kopfermann, *Nuclear Moments* (Academic, New York, 1958).

[9] W. H. King, *Isotope Shifts in Atomic Spectra* (Plenum, New York, 1984).

[10] P. Aufmuth, K. Heilig, and A. Steudel, At. Data Nucl. Data Tables **37**, 455 (1987).

[11] P. Aufmuth and M. Haunert, Physica B & C **123C**, 109 (1983).

[12] F. Schneider, P.h.D. thesis, Freie Universität Berlin, 1985.

[13] H. Geisen, T. Krumpelmann, D. Neuschafer, and Ch. Ottinger, Phys. Lett. A **130**, 299 (1988).

[14] K. Yoshino and D.E. Freeman, J. Opt. Soc. Am. B **2**, 1268 (1985).

[15] R.D. Knight and L.-G. Wang, J. Opt. Soc. Am. B **2**, 1084 (1985).

[16] C.J. Humphreys and E. Paul, Jr., J. Opt. Soc. Am. B **60**, 1302 (1970).

[17] D.A. Jackson and M.C. Coulombe, Proc. R. Soc. London, Ser. A **343**, 453 (1975).

[18] D.A. Jackson and M.C. Coulombe, Proc. R. Soc. London, Ser. A **338**, 277 (1974).